International Journal of Biological Macromolecules 51 (2012) 209–214

Contents lists available at SciVerse ScienceDirect

International Journal of Biological Macromolecules

journal homepage: www.elsevier.com/locate/ijbiomac

Crystallographic portrayal of different conformational states of a Lys49 phospholipase A_2 homologue: Insights into structural determinants for myotoxicity and dimeric configuration

A. Ullah[a], T.A.C.B. Souza[b], C. Betzel[c], M.T. Murakami[b], R.K. Arni[a,*]

[a] Centro Multiusuário de Inovação Biomolecular, Departamento de Física, Universidade Estadual Paulista (UNESP), São José do Rio Preto-SP, 15054-000 SP, Brazil
[b] Laboratório Nacional de Biociências, Centro Nacional de Pesquisa em Energia e Materiais, Campinas, 13083-970 SP, Brazil
[c] Institute of Biochemistry and Molecular Biology, University of Hamburg, Laboratory of Structural Biology of Infection and Inflammation, c/o DESY, Notkestrasse 85, Build. 22a, D-22603 Hamburg, Germany

ARTICLE INFO

Article history:
Received 13 March 2012
Received in revised form 28 April 2012
Accepted 5 May 2012
Available online 11 May 2012

Keywords:
Lys49 phospholipase A_2 homologue
Bothrops brazili
Tetraethylene glycol
Conformational states
Oligomerization

ABSTRACT

Catalytically inactive phospholipase A_2 (PLA_2) homologues play key roles in the pathogenesis induced by snake envenomation, causing extensive tissue damage via a mechanism still unknown. Although, the amino acid residues directly involved in catalysis are conserved, the substitution of Asp49 by Arg/Lys/Gln or Ser prevents the binding of the essential calcium ion and hence these proteins are incapable of hydrolyzing phospholipids. In this work, the crystal structure of a Lys49-PLA_2 homologue from *Bothrops brazili* (MTX-II) was solved in two conformational states: (a) native, with Lys49 singly coordinated by the backbone oxygen atom of Val31 and (b) complexed with tetraethylene glycol (TTEG). Interestingly, the TTEG molecule was observed in two different coordination cages depending on the orientation of the nominal calcium-binding loop and of the residue Lys49. These structural observations indicate a direct role for the residue Lys49 in the functioning of a catalytically inactive PLA_2 homologue suggesting a contribution of the active site-like region in the expression of pharmacological effects such as myotoxicity and edema formation. Despite the several crystal structures of Lys49-PLA_2 homologues already determined, their biological assembly remains controversial with two possible conformations. The extended dimer with the hydrophobic channel exposed to the solvent and the compact dimer in which the active site-like region is occluded by the dimeric interface. In the MTX-II crystal packing analysis was found only the extended dimer as a possible stable quaternary arrangement.

1. Introduction

Phospholipases A_2 (PLA_2s) represent the major venom component of snakes belonging to genus *Bothrops* and exhibit a broad range of biological effects including neurotoxicity, myotoxicity, cardiotoxicity, hemolysis, anticoagulant and antiplatelet activities [1–4]. Snake venom PLA_2s are classified into two main subgroups based on the presence of an aspartic acid residue at position 49 in the catalytically active Asp49-PLA_2 enzymes, or a lysine in homologues (Lys49-PLA_2s; reviewed in [5–7]) that are considered to be catalytically inactive due to their inability to hydrolyze natural phospholipids [8]. Other substitutions such as arginine at position 49 have been observed in the catalytically inactive PLA_2 homologue from *Zhaoermia mangshanensis* venom [9–11].

In spite of the fact that Lys49-PLA_2 homologues are catalytically inactive, they induce a strong myonecrotic effect that is independent of phospholipid hydrolysis or arachidonic acid pathway [12–14]. A number of models have been proposed to account for the molecular basis of their pharmacological activities; however the structural determinants remain elusive [10,11,14–21]. Lys49-PLA_2 homologues have also been implicated in the inhibition of the vascular endothelial growth factor [22] and exhibit broad antibacterial activities [23,24], indicating their clinical and biomedical relevance.

Bothrops brazili snake is widely distributed in Brazil and its venom contains two PLA_2s [25]; myotoxin-I (MTX-I, Asp49) and myotoxin-II (MTX-II, Lys49). MTX-II, which is enzymatically inactive, induces strong myonecrosis and dose-time dependent edema [26]. This toxin also display cytotoxic activity on human T-cell leukemia (JURKAT) lines and microbicidal effects against *Escherichia coli*, *Candida albicans* and *Leishmania* sp. [25]. In order to shed light on the molecular basis for the biological effects of MTX-II, its crystal structure was determined at 2.7 Å resolution providing details of the dimeric configuration and the role of the Lys49 residue in the coordination of ligands, which suggests an important

* Corresponding author at: Departamento de Física, Universidade Estadual Paulista (UNESP), São José do Rio Preto, 15054-000 SP, Brazil.
Tel.: +55 17 3221 2460; fax: +55 17 3221 2247.
E-mail address: arni@sjrp.unesp.br (R.K. Arni).

0141-8130/$ – see front matter © 2012 Elsevier B.V. All rights reserved.
http://dx.doi.org/10.1016/j.ijbiomac.2012.05.006

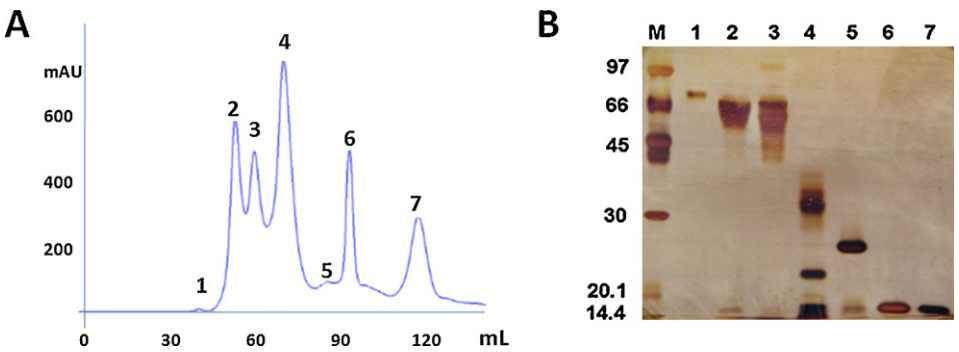

Fig. 1. (A) Molecular size-exclusion chromatographic profile of crude venom of *B. brazili*. (B) SDS-PAGE analysis of peaks from molecular size-exclusion chromatography. M: molecular weight markers (kDa), Lane 1; peak 1, Lane 2; peak 2, Lane 3; peak 3, Lane 4; peak 4, Lane 5; peak 5, Lane 6; peak 6, Lane 7; peak 7. Lane 6 represents the purified MTX-II.

contribution of the active site–like region in the expression of biological activities.

2. Materials and methods

2.1. Purification

Crude desiccated *B. brazili* venom was purchased from Serpentarium SANMARU Ltda, Taquaral, São Paulo, Brazil. 100 mg of this sample was suspended in a 1.5 ml solution (0.02 M Tris; 0.15 M NaCl, pH 8.0) and centrifuged at 10,000 × *g* for 10 min. The clear supernatant (1 ml) was applied into a 16 cm × 60 cm Sephacryl S-100 column previously equilibrated with the same buffer and eluted at a flow rate of 0.2 ml min^{-1} (Fig. 1A). All fractions were analyzed by sodium dodecyl sulfate-polyacrylamide gel electrophoresis [27] (Fig. 1B).

2.2. Dynamic light scattering

DLS measurements were performed on a Dynapro Molecular Sizing instrument at 291 K. The samples were previously centrifuged for 20 min at 20,000 × *g* and then, illuminated with laser of 1 μm (diameter) and the intensity fluctuations from the scattered light were measured in a 1 cm path length quartz cell. The data were collected with intervals of 10 s with at least 100 acquisitions. The diffusion coefficient (D_T) was determined from the decay rate distribution of intensity correlation profiles and used to calculate the hydrodynamic radius (R_h) of the protein via Stokes–Einstein equation ($D_T = k_b T(6\pi\eta R_h)^{-1}$, where T is the temperature in Kelvin, k_b is the Boltzmann's constant and η is the solvent viscosity). Analysis was performed using the software Dynamics V6.3.40.

2.3. Crystallization

The MTX-II sample was concentrated to 15 mg ml^{-1} in microconcentrators (AMICON) and crystallization was performed by the hanging-drop vapor-diffusion method at 291 K using 24-well tissue-culture plates [28]. The sample was screened against commercially available crystallization kits including crystal screen 1 and 2, grid screen ammonium sulfate and grid screen polyethylene glycol (PEG) 6000 (Hampton Research). Typically, 1 μl of protein solution was mixed with an equal volume of the screening solution and equilibrated over a reservoir containing 0.5 ml of the crystallizing solution. Initial tests yielded micro-crystals in the condition consisting of 0.1 M Tris–HCl pH 8.5, 0.2 M $MgCl_2$ and 18% (w/v) PEG 4000. This condition was optimized and single crystals adequate for X-ray diffraction were obtained when a 2 μl protein droplet was mixed with an equal volume of reservoir solution containing 0.1 M Tris pH 8.2, 25% (w/v) PEG 4000 (Fig. 2).

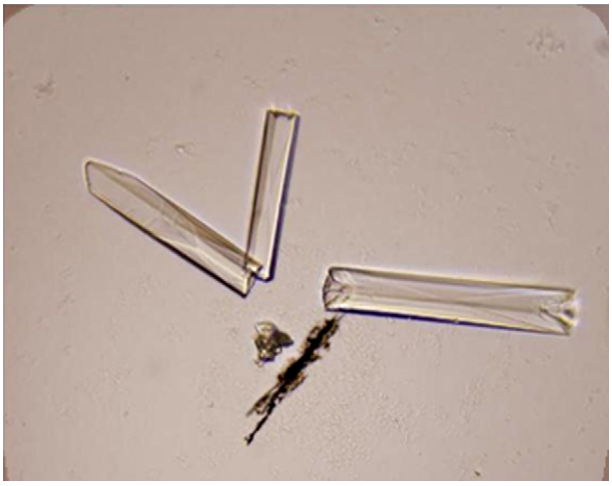

Fig. 2. Photomicrograph of MTX-II (maximum dimension: 200 μm).

2.4. Data collection, processing and structure determination

A MTX-II crystal was flash-cooled in a 100 K nitrogen-gas stream and X-ray diffraction data were collected on the W01B-MX2 beamline at the Brazilian Synchrotron Light Laboratory (LNLS-Campinas, Brazil). The wavelength of the radiation source was set to 1.458 Å and a MarMosaic 225 mm CCD detector was used to record the intensities. The crystal was exposed for 90 s with a rotation of 2° per frame and a total of 90 images were collected using a sample-to-detector distance of 100 mm. The data were indexed, integrated and scaled using the programs DENZO and SCALEPACK from the HKL-2000 package [29]. Data-processing statistics are presented in Table 1. Molecular replacement was carried out using the program MOLREP [30] and a model based on the atomic coordinates of bothropstoxin-I from *Bothrops jararacussu* (PDB ID: 2H8I [10]). The structure factors and atomic coordinates were deposited in the Protein Data Bank under the accession code 4DCF.

3. Results and discussion

3.1. Purification

An efficient and rapid procedure was established to purify the MTX-II from *B. brazili* venom, which encompasses a single size-exclusion chromatography on an S-100 Sephacryl column (Fig. 1A). The protein was obtained with purity higher than 95% (Fig. 1B) and yielded 10 mg of the protein from an initial amount of 100 mg of crude venom. Under denaturing conditions, the purified MTX-II migrated as a single protein band corresponding to a molecular

Table 1
Data collection and refinement statistics.

Data collection	
Temperature (K)	100
Radiation source	Brazilian Synchrotron Light Laboratory
Beamline	W01B-MX2
Wavelength (Å)	1.458
Detector	MarMosaic 225 mm
Space group	*C121*
Unit-cell parameters (Å,°)	$a = 59.4$, $b = 128.88$, $c = 67.0$; $\alpha = \gamma = 90.0$, $\beta = 105.66$
Resolution range (Å)	19.72–2.70
R_{merge}[a] (%)	11.6 (33.9)
$\langle I/\sigma(I)\rangle$	8.1 (2.6)
Data completeness (%)	94.2 (86.1)
Redundancy	3.0 (2.7)
Number of measured unique reflections	12,516
Data analysis	
V_M (Å^3 Da^{-1})	2.21
Solvent content (%)	44.26
Molecules per asymmetric unit	4
Model refinement	
Resolution range (Å)	19.72–2.70
R_{free} (%)	31.98
R_{factor} (%)	26.27
Number of reflections used in refinement	11,881
Number of protein atoms	3843
Water molecules	108
Ligands	2
R.m.s bond-length deviation (Å)	0.012
R.m.s bond-angle deviation (%)	1.472
Mean B-factor (Å^2)	36.95
Ramachandran plot analysis	
Most favored regions (%)	85
Allowed region (%)	15
Disallowed region (%)	0

[a] $R_{merge} = \sum_{hkl}\sum_i |I_i(hkl) - \langle I(hkl)\rangle| / \sum_{hkl}\sum_i I_i(hkl)$, where $I_i(hkl)$ is the ith observation of reflection hkl and $\langle I(hkl)\rangle$ is the weighted average intensity for all observations I of reflection hkl.

mass of 14 kDa, which is in a good agreement with the calculated value (13.7 kDa).

3.2. Structural description

MTX-II was sequenced and characterized by 25 and 26, respectively. The sequence comprises all the features of inactive Lys49-PLA$_2$ homologues including the residues Leu5, Gln11, Asn28, Leu32 and Lys49. Sequence alignment of MTX-II with other *Bothrops* Lys49-PLA$_2$ homologues indicated that the putative catalytic apparatus (catalytic triad + Tyr73) is fully conserved as well as the nominal calcium-binding loop. The most variable region is the C-terminus that may have a key role in myotoxicity [31–34].

The structure of MTX-II was solved at 2.7 Å resolution (Table 1) by molecular replacement using the atomic coordinates of bothropstoxin-I from *B. jararacussu* (PDB ID: 2H8I [10]) as a template. The atomic model displayed good overall stereochemistry with RMSD values of 0.012 Å and 1.472° for bond lengths and angles, respectively. The average temperature factor (B-value) for all atoms is 36.95 Å^2 (Table 1) and 85.0% of the dihedral angles are situated in the most favored regions, whereas the remaining 15.0% of residues are found in either permitted or generously allowed regions of the Ramachandran plot (Table 1). The asymmetric unit consists of two dimers related by a two-fold axis of rotation.

The molecular topology of MTX-II conserves all the main features of its homologues (Fig. 3A): the N-terminal α-helix H1 (residues Ser1–Thr13); the short helical turn (residues Pro17–Tyr21); the two long anti-parallel disulfide-linked α-helices H2 (residues Ala39–Lys57) and H3 (residues Ser90–Glu108) that are separated by 9 Å; the β-wing motif (residues Ser74–Gly86) and the flexible C-terminal region (Leu110-Cys133). The β-wing region is structurally conserved and is stabilized by two salt bridges (Asp79A–Arg107B and Lys80A–Glu12B) between the subunits forming the dimer of the asymmetric unit. Although stabilized by two disulfide bonds (Cys50-Cys133; Cys27-Cys127), the C-terminal region of MTX-II displays high flexibility as observed by B-factors values (Fig. 3B) likely due to the substitution of a conserved tyrosine by asparagine (residue 117) and the different conformational states observed for Lys122.

3.3. Lys49 coordination and its role in the stabilization of tetraethylene glycol

The active site-like region of Lys49-PLA$_2$ homologues is formed by His48, Lys49, Tyr52, Tyr73 and Asp99, and the catalytic water molecule. The residues Gly28, Gly29, Arg32 and Gly33 are involved in the coordination of Ca^{2+} ion in Asp49-PLA$_2$s [35–38], which plays a role in the stabilization of the tetrahedral intermediate during catalysis. In Lys49-PLA$_2$ homologues, the Lys49-NZ atom is located at the position of the Ca^{2+} ion and is coordinated by the backbone atoms from the CGVG/LGR motif.

In the MTX-II structure, the two dimers forming the asymmetric unit display different conformational states due to the presence of tetraethylene glycol (TTEG) bound to the dimer formed by molecules A and B. In the case of the second dimer formed by molecules C and D where the active site-like region is empty, the Lys49 side-chain is mono-coordinated by the carbonyl oxygen atom of Val31 (Fig. 4A). In molecule B, a TTEG molecule is found at the active site-like region and it is stabilized by a single hydrogen bond formed between its terminal hydroxyl group and Gly30 (Fig. 4B). In molecule A, TTEG is anchored to the nominal calcium-binding loop by the backbone of Gly30 analogously to molecule B and additionally by the NZ atom of Lys49, suggesting a contribution of Lys49 in the functioning of Lys49-PLA$_2$ homologues (Fig. 4C). In BthTX-I structure, a PEG fragment was also encountered bound to the active site-like region, conserving the hydrogen bond with Gly30 and making water-mediated interactions with His48 [10]. Fatty acids [39,40] and stearic acid [41] were also observed at the active site-like region of other Lys49-PLA2 homologues, which supports the importance of this interface for the expression of their pharmacological activities including myonecrosis and edema formation.

A correlation between the presence of the ligand at the active site-like region and the coordination of Lys49 was observed in the MTX-II structure. When Lys49 participates in the stabilization of TTEG, the carbonyl oxygens of Asn28 and Val31 are coordinated by the Lys49 side-chain, whereas in the unbound state Lys49 coordination is done by the carbonyl oxygens of Val31 and Gly33. These conformational changes in the nominal calcium-binding loop reflect in a rearrangement of the C-terminal region, which modifies the polarization and surface hydrophobicity.

The observed coordination modes of the Lys49 residue contrast with those already described for other Lys49-PLA$_2$ homologues, wherein the NZ atom is generally tri-coordinated by the backbone of atoms of residues Asn28, Gly30 and Gly33 [20]. In the Arg49-PLA$_2$ homologue, the substitution of Lys49 by Arg results in the dual coordination of the Arg49NH1 atom by Asn28 and Glu33 carbonyl oxygens and mono-coordination of the Arg49NH2 atom by the backbone of the residue Gly30, still preserving the triple coordination by the canonical residues.

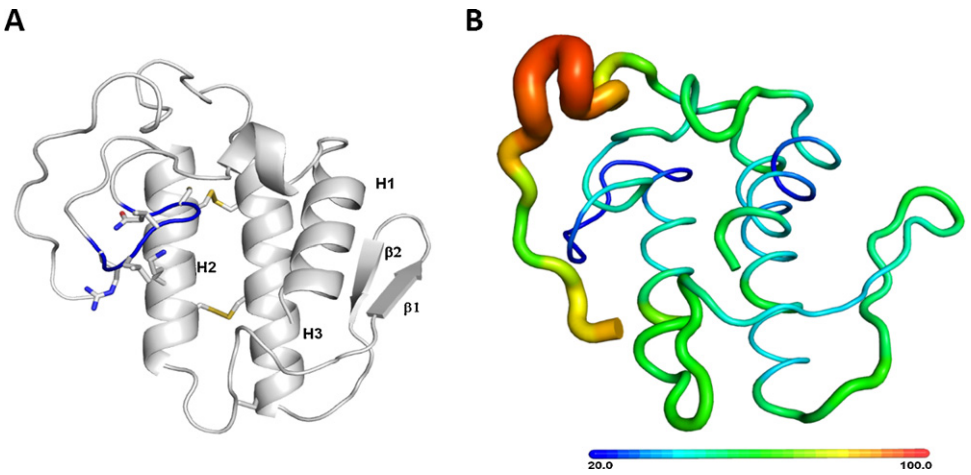

Fig. 3. (A) Overall structure of MTX-II. N-terminal α-helix H1 (residues Ser1–Thr13); one short helical turn (residues Pro17–Tyr21); the two long anti-parallel disulfide-linked α-helices H2 (residues Asp39-Lys57) and H3 (residues Ser90-E108) that are separated by 9 Å; the β-wing region (residues Ser74–Gly85) and the flexible C-terminal region (Leu110-Cys133). Nominal calcium binding loop are in blue. (B) MTX-II flexibility. Ribbon representation colored by B-factor. (For interpretation of the references to color in this figure legend, the reader is referred to the web version of this article.)

3.4. Unpolarized state of the C-terminal region in the presence of ligands

Different mechanisms have been proposed to the myonecrotic activity of Lys49-PLA_2 homologues related to their dimeric conformation [6,10,42] and formation of the hydrophobic knuckle [40]. In the latter model, the hyperpolarization of the peptide bond between residues Cys29 and Gly30 due to the presence of Lys122 causes a local rearrangement of the C-terminal residues (Fig. 4D). This is then locked into a conformation with the hydrophobic residues, Phe121 and Phe124 forming a hydrophobic knuckle that is exposed to the solvent and is considered essential for interaction with the membrane (Fig. 4D). However, in the MTX-II structure, the presence of tetraethylene glycol interacting with the nominal calcium-binding loop and Lys49 does not result in the formation of the hydrophobic knuckle. Analogously to MTX-II, the Zhaoermiatoxin (Arg49-PLA_2) in complex with a ligand also exhibits a C-terminal conformation where the hydrophobic residues are not

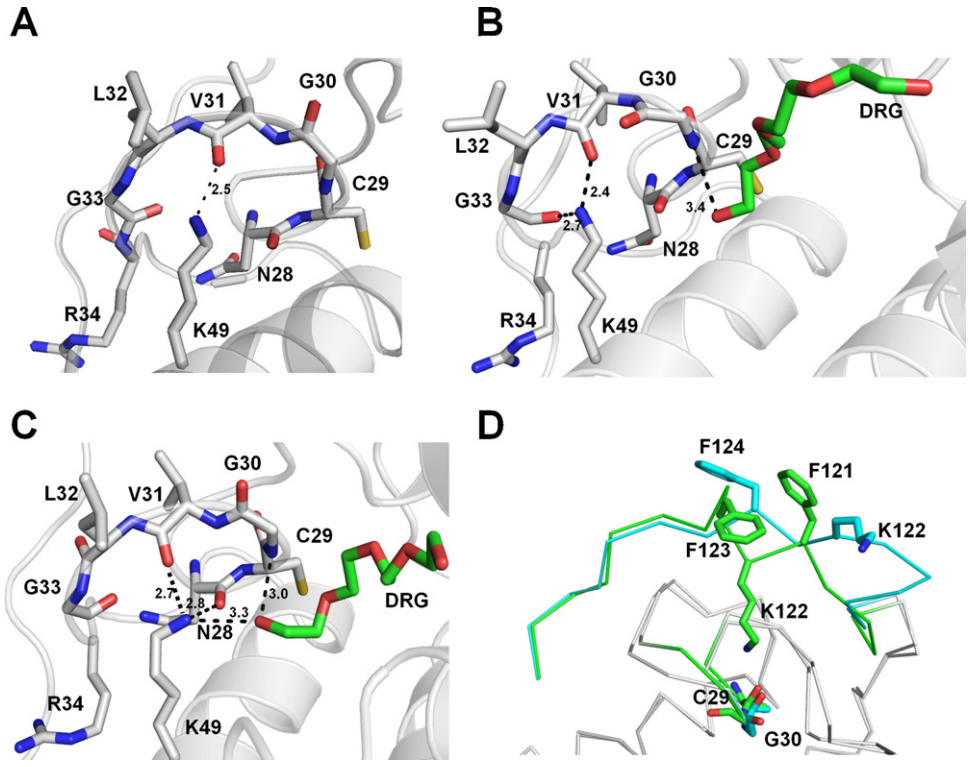

Fig. 4. (A) Relaxed conformational state of molecules C and D of MTX-II, where the Lys49 side-chain is mono-coordinated by carbonyl oxygen of Val31. (B) In the molecule B, the tetraethylene glycol (green) is only stabilized by Gly30 amide bond. (C) The molecule A of MTX-II with tetraethylene glycol (green) anchored to the nominal calcium-binding loop by the backbone of Gly30 and by the Lys49NZ atom. (D) Comparison of the unpolarized state of the C-terminal region in the presence of ligands (MTX-II, blue) with the hyperpolarized state of the Lys49-PLA_2 homologue from *Agkistrodon contortrix* (green). The presence of Lys122 in the active site hyperpolarizes the amide bond between residues Cys29 and Gly30 (carbon atoms in green). In MTX-II structure, Lys122 displays a different conformation (carbon atoms in blue). (For interpretation of the references to color in this figure legend, the reader is referred to the web version of this article.)

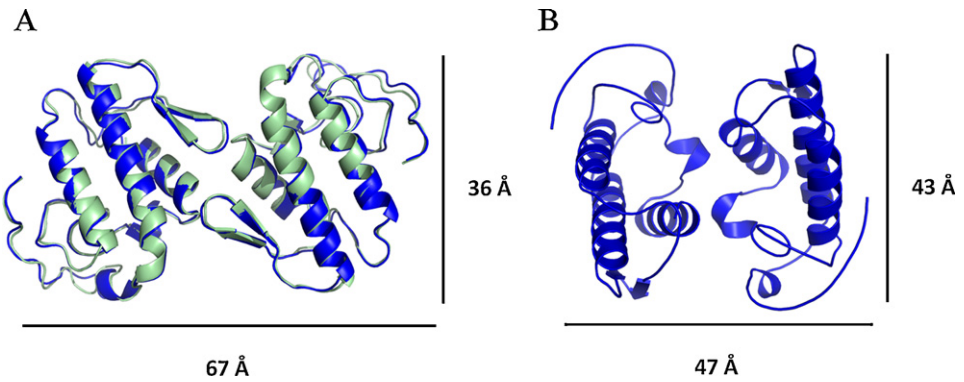

Fig. 5. Dimeric configuration of Lys49-PLA_2 homologues. (A) Extended dimer of MTX-II. (B) Compact dimer of BthTX-I (PDB ID: 2H8I).

exposed to the solvent. These results show that Lys49-PLA_2 homologues undergo structural rearrangements in the C-terminus when the active site-like region is occupied, providing new insights into their molecular mechanisms.

3.5. Oligomerization

All Lys49-PLA_2 homologues are characterized as dimers in solution and two dimeric configurations have been proposed for Lys49-PLA_2 homologues; an extended and a compact conformation [10,18,43] (Fig. 5). In the extended dimer, formed by hydrogen bonds between the β-wings, the hydrophobic channel and active-site cleft are exposed to the solvent [18,43], forming a common, large hydrophobic surface enabling the interaction with membranes. In the compact dimer, non-polar contacts predominate and the hydrophobic surface surrounding the PLA_2-active site-like regions are shielded from the solvent [10,20]. To date, all Lys49-PLA_2 homologue structures available in the Protein Data Bank can be interchangeably assembled in the two possible configurations. SAXS studies and crystal structure of several ligand complexes have been indicating the compact dimer as the biological assembly for Lys49-PLA_2 homologues.

DLS experiments also confirmed the dimeric state of MTX-II (results not shown) and crystal packing analysis showed that only the extended dimer can be formed using all possible symmetry operations. This is the unique crystal structure in which the compact dimer cannot be assembled by symmetry operations, suggesting that structural rearrangements by the presence of ligand could induce a switch between these two possible conformations or simply indicates that the extended dimer is the more likely biological unit of Lys49-PLA_2 homologues.

Authors' contributions

AU purified and crystallized the protein. TACBS and MTM collected X-ray diffraction data and refined the structure. CB and RKA analyzed the data, wrote the manuscript and supervised the project.

Acknowledgments

This research was supported by grants from CNPq, TWAS, FAPESP, DAAD and CAPES.

References

[1] S. Chwetzoff Tsunasawa, F. Sakiyama, A. Menez, Nigexine, Journal of Biological Chemistry 22 (1989) 13289–13297.
[2] R.M. Kini, Toxicon 45 (2005) 1147–1161.
[3] R.H. Schaloske, E.A. Dennis, Biochimica et Biophysica Acta 1761 (2006) 1246–1259.
[4] T.S. Kang, D. Georgieva, N. Genov, M.T. Murakami, M. Sinha, R.P. Kumar, P. Kaur, S. Kumar, S. Dey, S. Sharma, A. Vrielink, C. Betzel, S. Takeda, R.K. Arni, T.P. Singh, R.M. Kini, FEBS Journal 278 (2011) 4544–4576.
[5] R.K. Arni, R.J. Ward, Toxicon 341 (1996) 827–841.
[6] M.T. Murakami, R.K. Arni, Toxicon 42 (2003) 903–913.
[7] B. Lomonte, Y. Angulo, L. Calderón, Toxicon 42 (2003) 885–901.
[8] C.J. Van den Berg, A.J. Slotboom, H.M. Verheij, G.H. de Haas, Journal of Cellular Biochemistry 39 (1989) 379–390.
[9] D. Mebs, U. Kuch, F.I. Coronas, C.V. Batista, A. Gumprecht, L.D. Possani, Toxicon 47 (2006) 797–811.
[10] M.T. Murakami, M.M. Vicoti, J.R. Abrego, M.R. Lourenzoni, A.C. Cintra, E.Z. Arruda, M.A. Tomaz, P.A. Melo, R.K. Arni, Toxicon 49 (2007) 378–387.
[11] M.T. Murakami, U. Kuch, C. Betzel, D. Mebs, R.K. Arni, Toxicon 51 (2008) 723–735.
[12] B. Lomonte, A. Tarkowski, L.A. Hanson, Inflammation 17 (1993) 93–105.
[13] B. Lomonte, J. Lundgren, B. Johansson, U. Bagge, Toxicon 32 (1994) 41–55.
[14] B. Lomonte, E. Moreno, A. Tarkowski, L.A. Hanson, M. Maccarana, Journal of Biological Chemistry 269 (1994) 29867–29873.
[15] R.M. Kini, S. Iwanaga, Toxicon 24 (1986) 895–905.
[16] R.M. Kini, H.J. Evans, Biochemistry 28 (1989) 9209–9216.
[17] H.S. Selistre de Araujo, S.P. White, C.L. Ownby, Archives of Biochemistry and Biophysics 326 (1996) 21–30.
[18] R.J. Ward, A. Rodrigues Alves, J. Rugiero Neto, R.K. Arni, J.A. Casari, Protein Engineering 11 (1998) 285–294.
[19] S.H. Andriao-Escarso, A.M. Soares, V.M. Rodrigues, Y. Angulo, C. Diaz, B. Lomonte, J.M. Gutiérrez, J.R. Giglio, Biochimie 82 (2000) 755–763.
[20] M.T. Murakami, E.Z. Arruda, P.A. Melo, A.B. Martinez, S. Calil-Eliás, M.A. Tomaz, B. Lomonte, J.M. Gutiérrez, R.K. Arni, Journal of Molecular Biology 350 (2005) 416–426.
[21] M.T. Murakami, C.C. Melo, Y. Angulo, B. Lomonte, R.K. Arni, Acta Crystallographica Section F: Structural Biology and Crystallization Communications 62 (2006) 423–426.
[22] Y. Yamazaki, Y. Matsunaga, Y. Nakano, T. Morita, Journal of Biological Chemistry 280 (2005) 29989–29992.
[23] L. Paramo, B. Lomonte, J. Pizarro-Cerda, J.A. Bengoechea, J.P. Gorvel, E. Moreno, European Journal of Biochemistry 253 (1998) 452–461.
[24] C. Santamarıa, S. Larios, Y. Angulo, J. Pizarro-Cerda, J.P. Gorvel, E. Moreno, B. Lomonte, Toxicon 45 (2005) 807–815.
[25] T.R. Costa, D.L. Menaldo, C.Z. Oliveira, N.A. Santos-Filho, S.S. Teixeira, A. Nomizo, A.L. Fuly, M.C. Monteiro, B.M. de Souza, M.S. Palma, R.G. Stábeli, S.V. Sampaio, A.M. Soares, Peptides 10 (2008) 1645–1656.
[26] S. Huancahuire-Vega, L.A. Ponce-Soto, D. Martins-de-Souza, S. Marangoni, Toxicon 54 (2009) 818–827.
[27] U.K. Laemmli, Nature 227 (1970) 680–685.
[28] J. Jancarik, S.H. Kim, Journal of Applied Crystallography 24 (1991) 409–411.
[29] Z. Otwinowski, W. Minor, Macromolecular Crystallography Part A, Academic Press, 1997, pp. 307–326.
[30] A. Vagin, A. Teplyakov, Journal of Applied Crystallography 30 (1997) 1022–1025.
[31] B. Lomonte, J. Pizarro-Cerdá, Y. Angulo, J.P. Gorvel, E. Moreno, Biochimica et Biophysica Acta 1461 (1999) 19–26.
[32] C.E. Núñez, Y. Angulo, B. Lomonte, Toxicon 39 (2001) 1587–1594.
[33] B. Lomonte, Y. Angulo, C. Santamaría, Toxicon 42 (2003) 307–312.
[34] V. Núñez, V. Arce, J.M. Gutiérrez, B. Lomonte, Toxicon 44 (July (1)) (2004) 91–101.
[35] R.K. Arni, M.R. Fontes, C. Barberato, J.M. Gutiérrez, C. Díaz, R.J. Ward, Archives of Biochemistry and Biophysics 366 (1999) 177–182.
[36] D.F. Ketelhut, M.H. de Mello, E.L. Veronese, L.E. Esmeraldino, M.T. Murakami, R.K. Arni, J.R. Giglio, A.C. Cintra, S.V. Sampaio, Biochimie 85 (2003) 983–991.
[37] M.T. Murakami, A. Gabdoulkhakov, N. Genov, A.C. Cintra, C. Betzel, R.K. Arni, Biochimie 88 (2006) 543–549.

[38] M.T. Murakami, M.R. Lourenzoni, E.Z. Arruda, M.A. Tomaz, M.M. Viçoti, J.R. Abrego, P.A. Melo, R.K. Arni, Protein and Peptide Letters 15 (2008) 1002–1008.
[39] W.H. Lee, M.H. Toyama, A.M. Soares, J.R. Giglio, S. Marangoni, I. Polikarpov, Acta Crystallographica Section D: Biological Crystallography 55 (1999) 1229–1230.
[40] A.L. Ambrosio, M.C. Nonato, H.S. de Araújo, R. Arni, R.J. Ward, C.L. Ownby, D.H. de Souza, R.C. Garratt, Journal of Biological Chemistry 280 (2005) 7326–7335.
[41] L.L. Watanabe, A.M. Soares, R.J. Ward, M.R. Fontes, R.K. Arni, Biochimie 87 (2005) 161–167.
[42] A.J. Magro,.M.T. Murakami, S. Marcussi, A.M. Soares, R.K. Arni, M.R. Fontes, Biochemical and Biophysical Research Communications 323 (2004) 24–31.
[43] M.T. da Silva-Giotto, R.C. Garrat, G. Oliva, Y.P. Mascarenhas, J.R. Giglio, A.C.O. Cintra, de W.F. Azevedo Jr., R.K. Arni, R.J. Ward, Proteins-Structure Function and Genetics 30 (1998) 442–454.